Materials Horizons

ROYAL SOCIETY OF CHEMISTRY

COMMUNICATION

View Article Online
View Journal | View Issue

Check for updates

Cite this: *Mater. Horiz.*, 2024, **11**, 969

Received 12th August 2023,
Accepted 21st November 2023

DOI: 10.1039/d3mh01280h

rsc.li/materials-horizons

Ductile adhesive elastomers with force-triggered ultra-high adhesion strength†

Xiao Zhao,[a] Zoriana Demchuk,[a] Jia Tian,[b] Jiancheng Luo,[a] Bingrui Li,[c] Ke Cao,[a] Alexei P. Sokolov,[ad] Diana Hun,*[e] Tomonori Saito*[ac] and Peng-Fei Cao*[b]

Elastomers play a vital role in many forthcoming advanced technologies in which their adhesive properties determine materials' interface performance. Despite great success in improving the adhesive properties of elastomers, permanent adhesives tend to stick to the surfaces prematurely or result in poor contact depending on the installation method. Thus, elastomers with on-demand adhesion that is not limited to being triggered by UV light or heat, which may not be practical for scenarios that do not allow an additional external source, provide a solution to various challenges in conventional adhesive elastomers. Herein, we report a novel, ready-to-use, ultra high-strength, ductile adhesive elastomer with an on-demand adhesion feature that can be easily triggered by a compression force. The precursor is mainly composed of a capsule-separated, two-component curing system. After a force-trigger and curing process, the ductile adhesive elastomer exhibits a peel strength and a lap shear strength of 1.2 $\times$ 10^4 N m^{-1} and 7.8 $\times$ 10^3 kPa, respectively, which exceed the reported values for advanced ductile adhesive elastomers. The ultra-high adhesion force is attributed to the excellent surface contact of the liquid-like precursor and to the high elastic modulus of the cured elastomer that is reinforced by a two-phase design. Incorporation of such on-demand adhesion into an elastomer enables a controlled delay between installation and curing so that these can take place under their individual ideal conditions, effectively reducing the energy cost, preventing failures, and improving installation processes.

[a] Chemical Sciences Division, Oak Ridge National Laboratory, Oak Ridge, TN 37830, USA. E-mail: saitot@ornl.gov

[b] State Key Laboratory of Organic–Inorganic Composites, Beijing University of Chemical Technology, Beijing 100029, China. E-mail: caopf@buct.edu.cn

[c] The Bredesen Center for Interdisciplinary Research and Graduate Education, University of Tennessee, Knoxville, TN 37996, USA

[d] Department of Chemistry, University of Tennessee, Knoxville, TN 37996, USA

[e] Buildings and Transportation Science Division, Oak Ridge National Laboratory, Oak Ridge, TN 37830, USA. E-mail: hunde@ornl.gov

† Electronic supplementary information (ESI) available. See DOI: **https://doi.org/10.1039/d3mh01280h**

New concepts

In this manuscript, we pioneer the incorporation of the unique ''on-demand'' adhesion feature into functional ductile elastomers, which is completely different from regular pressure-sensitive adhesives. The adhesion feature is easily triggered by mechanical force when needed, and such a feature can effectively reduce the energy cost, prevent damage and improve convenience during handling. After a force trigger and curing process, it exhibits a peel strength and a lap shear strength of 1.2 $\times$ 10^4 N m^{-1} and 7.8 $\times$ 10^3 kPa, respectively, which top the values reported for advanced functional adhesive elastomers. The rheological properties of the adhesive elastomer after curing reveal that the excellent ability to adapt to rough surfaces and the reinforced elastomer modulus contribute to the ultra-high adhesion strength. The unique ''on-demand'' adhesion of functional elastomers will shed light on fabricating functional polymeric materials with different applications.

1. Introduction

Elastomers are rooted in every aspect of our daily life as they are used in consumer and industrial products like sealants, vibration dampers, tires, footwear, toys, furniture, packaging, adhesives, additives, *etc.* They play a vital role in forthcoming advanced technologies, including but not limited to flexible displays, wearable devices, soft robotics, invasive surgery, building construction, solid-state batteries, and artificial human skin.[1–9] Chemical or physical crosslinking of natural rubber, polyurethane, polybutadiene, neoprene, co-polyester, or silicone-based polymers, allow ductile elastomers to possess properties like good extensibility, decent elastic modulus, remarkable recoverability (low mechanical loss), and excellent chemical resistance.[10–15] Aside from these fundamental properties, advanced ductile elastomers can have other special features such as self-healing, chemical stability, dielectric response, thermal or magnetic sensitivity, and high optical transparency. These features are typically accomplished by the introduction of single or multiple dynamic bonds, the addition of functional additives, formation of micro-phase separations, manipulation of molecular topology, or engineering into special geometry or composites.[16–33] For example, a graphene-containing liquid crystalline elastomer enabled photo-actuation by absorbing near-infrared light and triggering nematic-to-isotropic phase transition, achieving high actuation force and reversible flexibility.[22] The interpenetration of the conductive PEDOT:PSS and zwitterionic poly(HEAA-*co*-SBAA) networks allowed the fabrication of a fully polymeric strain sensor with high mechanical recovery and strong surface adhesion.[34] A super stretchable ($\approx$2260%) and recyclable polyurethane elastomer was recently achieved by introducing dynamic π–π motifs and phosphorus-containing moieties.[15] An ionic conducting elastomer with autonomous self-healability at 5 °C also serves as an efficient protecting layer for the stable cycling of lithium-metal batteries at relatively low temperatures.[35]

With significantly growing demands of functional ductile elastomers in advanced technologies, their adhesive properties play a critical role in determining their lifetime and reliability in the designated fields.[36–45] The incorporation of intermolecular interactions is an important strategy to improve the adhesive properties of elastomers. For example, Chen *et al.* and Tan *et al.* independently demonstrated that the incorporation of a small number of hydrogen-bonding 2-ureido-4[1*H*]-pyrimidinone (UPy) groups enhanced the adhesion force of the elastic materials to organic and inorganic substrates for finger strain sensors and soft robot actuators.[46,47] By using the monomer of 4-acryloyl morpholine that intrinsically possesses hydrogen-bonding interactions, a self-adhesive ionic elastomer was synthesized that exhibited a peel strength of 28 N m^{-1} on a paper substrate and allowed the assembly of stretchable motion energy harvester.[48] The addition of 15 mol% dopamine increased the adhesive strength of urethane elastomers from 30 to 71 kPa when used as bio-interfacial electrodes.[27] A series of self-healable, adhesive elastomers were also demonstrated to show ultra-high adhesion force, even on dusty surfaces (3488 N m^{-1}), by simply mixing the self-healing polymer and commercially available curable elastomers.[25] Aside from physical interactions, adjusting the surface geometries in the microscale also facilitates the adhesion of elastomers to various substrates. For example, the adhesion force of the poly(dimethyl siloxane) (PDMS) elastomer to the human skin was improved by 10 times due to the enhanced van der Waals force *via* the formation of micrometer-sized wrinkles on the elastomer, which was rendered by the addition of 0.004 wt% ethoxylated poly(ethyleneimine).[49] By controlling the interfacial interaction-induced surface wrinkling between poly(L-lactide) and PDMS, a single-component micro-wrinkled PDMS elastomer was shown to have tunable adhesion capabilities.[50] Although the enhancement of adhesion force has been demonstrated for functional ductile elastomers, few have the flexibility of the on-demand control when full-adhesion occurs. Therefore, they often require extra protection and labor before and during the installation onto the target substrate and lack convenience during handling. Hence, developing a force-triggered on-demand feature is a more practical, one-step solution for scenarios such as flexible devices or prefab construction that will significantly benefit from having a controlled delay between installation and adhesion.

Microencapsulation technology, which originated from the pursuit of a protective envelope that can control the exchange of materials such as a living cell, has been widely adopted in different applications such as extrinsic self-healing,[51–53] food protection,[54] drug delivery,[55] wound management,[56,57] photovoltaic protection,[58] thermal sensitive adhesives,[59] *etc.* In general, the active ingredients encapsulated in the micro shells are released continuously at a slow rate or completely upon shell rupture. The latter could be triggered by physical stimuli, such as macroscopic fracture,[51,60,61] temperature,[59,62] ultra-sound,[63] and compression.[64–66] Among the above, the compression force is the most convenient trigger, as no thermal or acoustic equipment is required. Also, it allows a universal breakage of microcapsules that triggers adhesion in comparison to the crack or fracture that only triggers local healing.

Herein, we demonstrate a novel design for an on-demand, ultra-high strength ductile adhesive elastomer, whose adhesion is triggered by compression force. This triggering method is more robust than the moisture or light-triggered curing, since such factors are normally difficult to avoid under ambient conditions.[67] In general, we selected a urea-based elastomer that is fabricated by methylene diphenyl diisocyanate (MDI)-prepolymer and polypropylene glycol (PPG)-diamine as resin and curing agents, respectively. The on-demand feature is achieved through a compression force to break the encapsulated resin agent and trigger the curing reaction, as illustrated in Fig. 1. Notably, our design is different from the two/multi-component self-healing,[51,60,61] of which our adhesive elastomer is homogenously cured with mechanical performance and interfacial binding significantly improved, whereas the micro-encapsulation-based self-healing aims at repeatedly restoring the local damage. Also, this adhesive elastomer is different from the conventional pressure-sensitive adhesives, as the latter involves merely physical tacking and typically low adhesion on rough surfaces as will be discussed later. Here, the combination of the intrinsic adaptability on the receiving substrate, *i.e.*, micro-scale geometry adaption, and the reinforced mechanical strength enabled the developed ductile adhesive elastomer to achieve an ultra-high adhesion force with peel strength and adhesion strength exceeding magnitudes of 10^4 N m^{-1} and 10^3 kPa, respectively. To the best of our knowledge, the adhesion force of such elastomers outperforms that of the currently reported ductile adhesive elastomers. With such ultra-high adhesion force and on-demand adhesion that can be conveniently applied by human force, it is anticipated that such ductile adhesive elastomer can be used in a large variety of applications.

2. Results and discussion

The ready-to-use elastomer precursor is composed of an encapsulated MDI-prepolymer and PPG-diamine, as reactive and curing agents, respectively, along with a matrix polymer of methyl methacrylate-butyl acrylate-ethylhexyl acrylate random copolymer poly(MMA-r-BA-r-EHA), as depicted in Fig. 1. The reactive

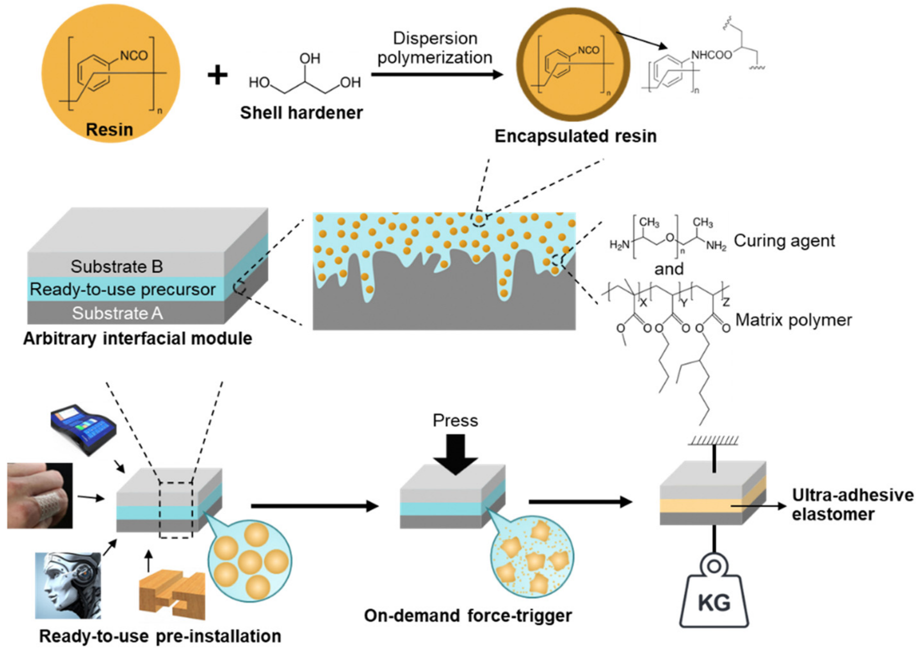

Fig. 1 Illustration of the on-demand ultra-high adhesion formation of the ready-to-use precursor and its preparation process. The resin, curing agent, and matrix polymer are MDI-prepolymer, PPG-diamine, and acrylates copolymer, respectively.

and curing agents were selected based on pre-screens of curing rate from various two-component elastomer systems, between a reactive agent, including bisphenol A diglycidyl ether, unsaturation-modified epoxy, hexamethylene diisocyanate (HDI) prepolymer, and MDI-prepolymer, and a curing agent, including polyethyleneimine (PEI), PPG-triamine, PPG-diamine, and PPG-di-OH.[68–70] A suitable curing rate allows adequate time for the substrates that will be adhered to each other to be adjusted while they did not require too long waiting time (<2 hours). The pre-screen tests (ESI,† Table S1) showed that neither diol- nor PEI-type curing agent cured at a reasonable rate. Additional PPG-triamine is required to slow down the PEI-type curing agent, which adds to the complexity. Regarding the reactive agents, the epoxy-based agents cured relatively slow with diamine/triamine, and HDI-prepolymer cured too fast with the diamine in which the additional diol is required for a suitable curing rate. Therefore, the combination of the MDI-prepolymer and PPG-diamine was the most suitable among them, considering their curing rate as well as the raw materials availability and the ability to be scaled up. Both the MDI-prepolymer and PPG-diamine contain reactive terminal groups with sufficient chain length to attain flexibility for the obtained elastomer without harming its cohesive strength.[71–73] The adhesive random copolymer, *i.e.*, poly(methyl methacrylate-*r*-butyl acrylate-*r*-2-ethylhexyl acrylate) was utilized as a polymer matrix, which improves the longevity and interfacial adhesion for the elastomers, especially before the force-triggered curing.

The microencapsulation process is established,[52,53] and the encapsulated MDI-prepolymer was synthesized using a single-step dispersion polymerization between MDI-prepolymer and glycerol, as illustrated in Fig. 1. Specifically, gum arabic, dodecyl trimethylammonium bromide (DTAB), and glycerol were used as the surfactant, segregation aid, and shell extender with the synthesis protocol demonstrated in Scheme S1 (ESI†). The well-dispersed MDI-prepolymer droplets were partially crosslinked by glycerol to form the shell of the microcapsules,[68] sealing the unreacted MDI-prepolymer inside. It is noteworthy that the addition of a cationic surfactant, *i.e.*, DTAB, introduces coulombic repulsion on the surface of the microcapsules that effectively prevents microcapsule aggregation (ESI,† Fig. S1), which increases the robustness of microcapsules during handling. The characteristic chemical structure of the shell was demonstrated by FT-IR as shown in Fig. 2A. The peaks at 1235 and 1310 cm^{-1} correspond to the urethane ester bond formed between isocyanate groups from MDI-prepolymer and hydroxyl units in glycerol.[74,75] Moreover, a significant peak at 2250 cm^{-1} that corresponds to the isocyanate group was observed for both broken microcapsules and MDI-prepolymers,[76] indicating the presence of a significant amount of reactive isocyanate groups inside the microcapsule. The DSC result (ESI,† Fig. S2) of the MDI-prepolymer-containing microcapsule also confirmed the presence of an isocyanate group. The diameter of the microcapsule was tunable from 10 to 900 μm by changing the mixing speed of the agitator during dispersion. The plot of microcapsule diameters *vs.* agitating speeds is provided in Fig. 2B, along with the representative optical microscope images for samples prepared at 300 and 1000 rpm. Tuning the size of microcapsules can potentially affect two important factors: (1) the force required to break the microcapsules and trigger the curing reaction; (2) the dispersion of released reactive agents in the polymer matrix. The scanning electron microscopy (SEM) images (ESI,† Fig. S3) clearly showed that the microcapsules can be broken by sufficient external force.

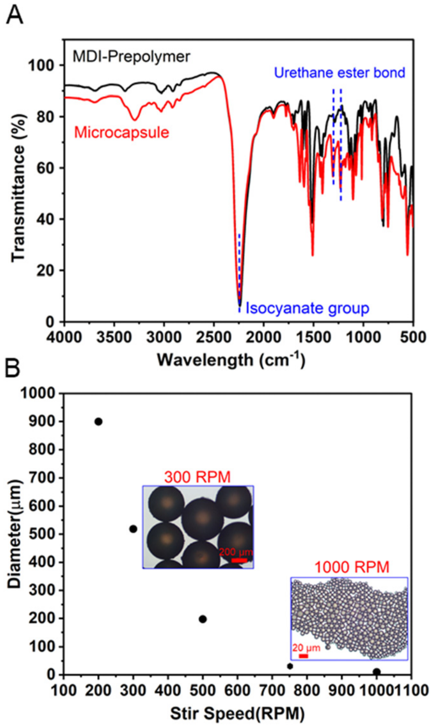

Fig. 2 (A) FT-IR spectra of MDI-prepolymer reagent and encapsulated MDI-prepolymer. (B) Diameter of the synthesized microcapsules *vs.* the agitation speed during emulsion polymerization, along with visualizations of the microcapsules by an optical microscope.

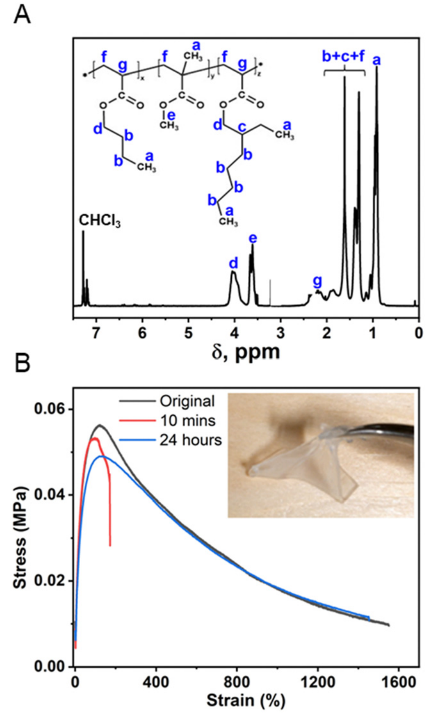

Fig. 3 (A) ^1H-NMR spectrum of the matrix polymer with characteristic chemical shift peaks marked on the chemical structure. (B) Tensile results of the cut matrix polymer that self-healed for 10 min and 24 h in comparison to the original uncut material.

The matrix polymer was synthesized by free-radical random copolymerization of methyl methacrylate (MMA), butyl acrylate (BA), and ethylhexyl acrylate (EHA).[77] The random copolymer with the feed ratio of MMA of 35 mol% was selected due to its suitable glass transition temperature (T_g), which optimized the adhesion and self-healability; the BA to 2-EHA feed ratio was 2 : 1 by weight. The chemical structure of the synthesized matrix polymer was confirmed by ^1H NMR (Fig. 3A) and FT-IR spectra (ESI,† Fig. S4), where the composition of the MMA unit was 29 mol%, as calculated by integrating the corresponding ^1H NMR peaks, consistent with the feed ratio. The molecular weight (M_n) of the copolymer was 23.6 kDa as measured by GPC, and the relatively broad polydispersity (PDI = 2.62) is typical for such random radical copolymerization. The low T_g (−33 °C using DSC, ESI† Fig. S5) manifested the rubbery nature of such copolymers over a wide temperature range. The dynamic mechanical analysis (DMA) result (ESI,† Fig. S6) clearly demonstrated that the modulus of the matrix polymer was around 2–5 MPa at room temperature, which is important for good interfacial adhesion. The tensile test exhibited excellent extensibility of such matrix polymer with elongation before breaks over 1500%. Having low T_g, high flexibility and adhesion also contributes to the self-healing capability. The self-healability was examined by mechanically cutting the cured adhesive into two parts and subsequently arranging them so that they were in contact with each other. After a 24 hour healing process under ambient conditions, the matrix polymer could fully recover its mechanical properties as shown in Fig. 3B.

The ready-to-use precursor was further formulated using the synthesized microcapsules with the encapsulated MDI-prepolymer, PPG-diamine, and matrix polymer. Specifically, we chose the microcapsules that were synthesized under 300 rpm for the following results. The initial formulation of the elastomer precursor contained 60 wt% microcapsules, 30 wt% PPG-diamine, and 10 wt% matrix polymer, which afforded the cured elastomer with adhesion force in the order of magnitude of 10^3 N m^{-1} (ESI,† Fig. S7). To optimize the composition ratios for the maximal reaction extent, the isocyanate content in the microcapsules with a diameter of 520 μm was calculated through titration using bromophenol and an excess quantity of amines (see Scheme S2, ESI† for the titration protocol). Based on the calculated result (isocyanate content 20.9 wt%), we optimized the composition of the ready-to-use precursor to be 50 wt% encapsulated MDI-prepolymer, 40 wt% PPG-diamine, and 10 wt% matrix polymer, so the unreacted excess agents were minimized. Such formulation was utilized for further studies.

To better control the force during the pre-installation process and on-demand curing, we loaded the precursor on to a customized shallow groove-shaped container. The curing reaction was then triggered by applying a 500 N compression force for 30 seconds on a 10 cm^2 flat surface, and such a short dwell time was sufficient to allow a homogeneous force distribution against the stress relaxation of the precursor. The 500 N compression force was selected based on the preliminary screening of the breaking state of microcapsules and the resultant peel strength (ESI,† Table S2, and Fig. S8) against different compression forces. A significant increase (500%) in peel strength was observed for 500 N, indicating sufficient breakage of microcapsules. Notably, this does not necessarily mean that all microcapsules were broken by such compression force, because there might be a small portion of smaller microcapsules requiring larger compression force. However, the amount of such a small portion was inadequate to cause significant macroscopic defects that influence the cohesive strength of the elastomer. Such a hypothesis was indirectly proven by similar tests for microcapsules synthesized at 200 rpm (Table S3 and Fig. S9, ESI†), where the critical inflection region became less steep due to the broader distribution of microcapsule size. On the other hand, the microcapsules synthesized at 200 rpm exhibit inferior adhesion performance compared to those at 300 rpm. The advantage of microcapsules synthesized at 200 rpm is that a lower trigger force, 150 N, was sufficient to trigger the curing. Obviously, the triggering force could be further tuned by varying the microcapsule sizes and adjusting the precursor formulation, whereas this fine-tuning confronted the challenge as the capsule thickness needed to be proportionally scaled against its size. After compression, the sample was cured for three days for complete cure at 25 °C in a temperature-controlled chamber prior to being processed for the tensile test (Fig. 4A). Herein, the tensile test was performed at a tensile rate of 1 mm s^{-1} with the result plotted in Fig. 4B. The cured elastomer illustrated a maximum tensile stress of 1.75 MPa and an elongation at breakage of 223%, a decent mechanical performance in comparison with advanced ductile adhesive elastomers.[48,49,78–81]

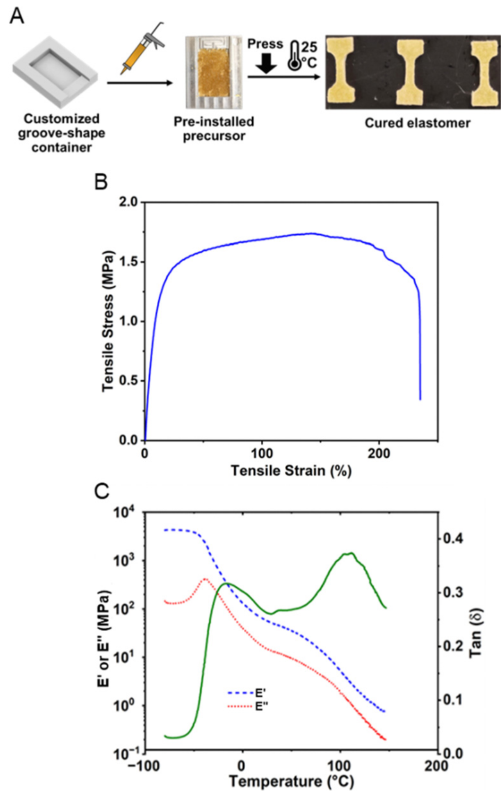

Fig. 4 (A) Protocols to cure the pre-installed precursor and preparation of samples for tensile tests. (B) Tensile result of the ductile adhesive elastomer that was cured at 25 °C for three days. (C) Dynamic modulus and phase angle of the cured ductile adhesive elastomer by temperature sweep using DMA.

The viscoelasticity of the cured elastomer was further investigated by temperature sweep using DMA as shown in Fig. 4C. At temperatures below −35 °C, a typical glassy modulus of around 4.3 GPa was observed. As the temperature increases, the result of the phase angle clearly indicates a broad transition from −25 °C to 0 °C, due to the devitrification of the cured ductile polyurea elastomer network. Herein, longer polyether chains were selected between crosslinks to avoid high rigidity, and therefore the T_g of the network was relatively low compared to rigid polyurea materials.[82] From 0 to 75 °C, a temperature-dependent elastic region was demonstrated for cured elastomers, mainly due to the strongly temperature-dependent mechanical strength of the matrix polymer. The characteristic elastic modulus is around 40 MPa, which is at least 10 times higher than the typical rubber-state modulus.[83–87] The high elastic modulus intrinsically enhances the cohesive strength of the adhesive elastomer.[88–91] Such enhancement was presumably caused by the mechanical reinforcement of the highly crosslinked microcapsule shells phase-separated in the elastomer matrix.[31,92–94] The existence of phase separation was indicated in the tan (δ) spectrum (Fig. 4C) as a high-temperature transition peak at 110 °C, and such temperature agreed with the T_g of crosslinked microcapsules (ESI,† Fig. S2).

As mentioned earlier, the novel design achieves the on-demand, ultra-high adhesion strength. The on-demand feature is important especially when the ductile adhesive elastomeric materials need a controlled delay between installation and adhesion, which often requires exterior protection and lacks flexibility of the installation. Some previous research (even current commercial products) have demonstrated the moisture- or light-triggered adhesion, although such triggering factors were easily disturbed by ambient humidity or light.[67] Conversely, the mechanical-force trigger can be easily controlled under ambient conditions and readily applied by end users. Herein, the on-demand feature is easily achieved by applying a uniform compression force on the pre-installed ready-to-use precursor. Such a strategy is different from the well-reported pressure-sensitive adhesives, although the latter also has an on-demand feature. The regular pressure-sensitive adhesives involve no chemical changes during installation, and the external force triggers a viscoelastic change to tack to the substrate. Therefore, its crosslinking extent and matrix rigidity are limited, as the peel strength is around 10^3 N m^{-1}.[95–97] Moreover, the thickness of pressure-sensitive adhesives is often less than 100 μm, to retain the shear resistance,[98–100] which limits its performance on various rough surfaces. In contrast, our force-triggering strategy involves a chemical curing process that provides at least 10 times higher strength to adhere to the substrate and maintain cohesion, as shown below. Moreover, the flexibility of the ready-to-use precursors and unlimited choices of thickness facilitate versatile adaptation with various surface conditions.

The adhesion force of the ductile adhesive elastomer was studied by the peel and lap shear strength to benchmark the reported ductile adhesive elastomers. Here, we used customized test kits that contain an embedded groove, similar to the container illustrated in Fig. 4A, and the testing methods comply with ASTM C794 and C961 standards. The test results of peel strength and lap shear on both aluminum and wood substrates, along with pictures of the testing setup, are shown in Fig. 5A and B. After curing at room temperature, the peel strength (tensile rate of 50 mm min^{-1}) was 1.2×10^4 N m^{-1} (294 N per inch) and 7.5×10^3 N m^{-1} (192 N per inch) for aluminum and wood substrates, respectively. The lap shear strength (tensile rate of 12.7 mm min^{-1}) was 2.1×10^3 and 7.8×10^3 kPa for aluminium and wood substrates, respectively. To the best of our knowledge, in terms of adhesion force, our on-demand ductile adhesive elastomer tops the reported advanced ductile adhesive elastomers as illustrated by a summary of adhesion performance *vs.* materials shown in Fig. 6.

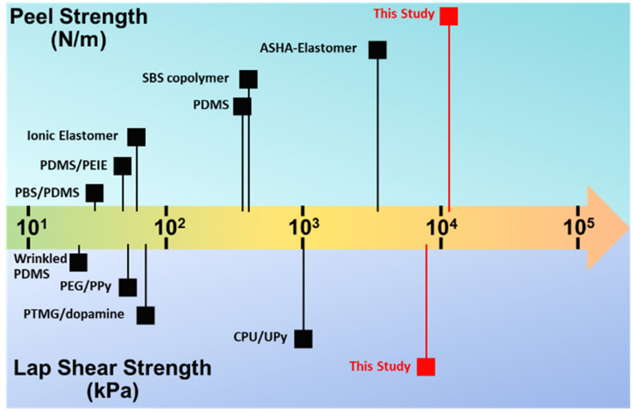

Fig. 6 Summary of adhesion performance of currently reported advanced ductile adhesive elastomers, including the reported chemistries: ASHA-elastomer,[25] SBS copolymer,[39] PDMS,[21] ionic elastomer,[48] PDMS/PEIE,[49] PBS/PDMS,[64] CPU/UPy,[47] PTMG/dopamine,[27] PEG/PPy,[46] and wrinkled PDMS.[50]

This ultra-high adhesion force provides a robust strategy to be utilized for applications on various substrate surfaces, and it can be explained by the following two reasons. First, the high mechanical robustness of the cured elastomer increases the cohesion strength. As measured by DMA, it showed an elastic modulus at least 10 times higher than regular rubbers, which provided reinforced cohesion during the peel test. Second, the ready-to-use precursor was pre-installed as a relatively liquid-like state that allowed the elastomer to adapt well to the texture roughness of the interface, significantly increasing the contact area. To examine the adhesion contribution from the matrix polymer, we also applied the peel test on the matrix polymer using the same abovementioned method. As shown in Fig. S10 (ESI†), the peel strength of the matrix polymer was only 1.8×10^3 N m^{-1} with clear cohesion failure observed (*vs.* 2.1×10^4 N m^{-1} for our ductile adhesive elastomer). These results confirm the advantage of such a unique design that has a soft nature for efficient contact during installation and is mechanically robust after a force-triggered curing reaction.

The on-demand adhesion feature has great potential for prefab construction,[101–103] as the precursor could be easily pre-installed at the prefab plant and triggered at the construction site when components are assembled, and hence effectively reducing assembly time and cost and improving installation quality and performance. To demonstrate the potential application,

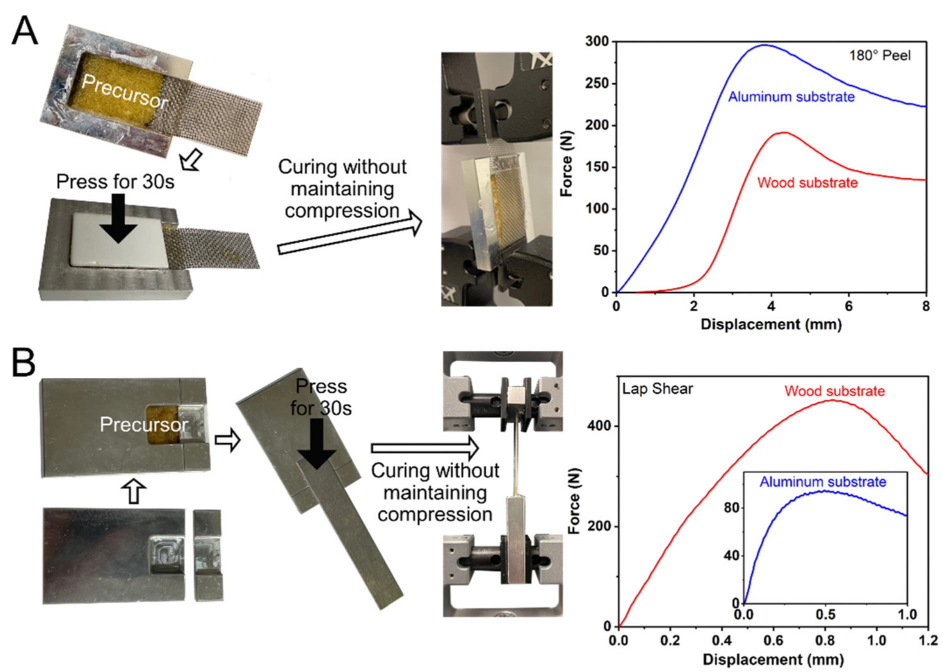

Fig. 5 (A) Peeling result of the cured ductile adhesive elastomer using a 180° peel setup. (B) Tensile result of the cured ductile adhesive elastomer using a lap shear setup.

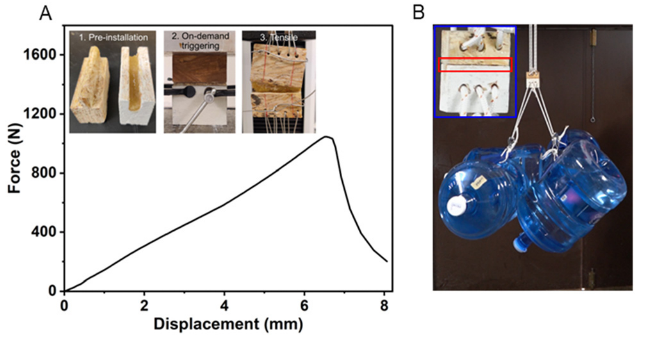

Fig. 7 (A) Tensile result of the bench-scale prefab joints connected by our cured elastomer, along with the protocol of setting up the bench-scale prefab joint. (B) Illustration of the ultra-high adhesion performance of our ductile adhesive elastomer using the bench-scale prefab joints.

we prepared an example of a prefab tongue and grove joint that is commonly used with wood sheathings or boards with our elastomer precursor (Fig. 7A). The joint was compressed for 30 seconds and cured under ambient conditions. Our high-resolution Instron tensile machine could barely pull the 5 cm-wide joints apart, as it exceeded the maximum load of 1000 N (Fig. 7A). The ultra-high adhesion force is further illustrated in Fig. 7B as the cured ductile adhesive elastomer could withstand the weight of 4 jugs of water, roughly 80 kg.

3. Conclusions

In summary, we report a novel design of ductile adhesive elastomers whose ultra-high adhesion strength can be easily triggered by an external force. The ready-to-use precursor was easily prepared with the encapsulated MDI-prepolymer as a reactive agent, PPG-diamine as the curing agent, and polyacrylates as a matrix polymer. The encapsulated MDI-prepolymer was synthesized by partially crosslinking the MDI-prepolymer and the diameter of the microcapsules was adjustable. The polyacrylate matrix polymer improved the adhesion of the precursor and provided the advantage of self-healability. The on-demand adhesion feature was achieved by pre-installing the precursor onto a surface and the feature was easily triggered by compression force. After curing, our ductile adhesive elastomer exhibited a peel strength and a lap shear strength of 1.2×10^4 N m^{-1} and 7.8×10^3 kPa, respectively, which tops the reported adhesion force for advanced ductile elastomers. This ultra-high adhesion force is mainly due to the excellent surface contact of the liquid-like precursor and the high elastic modulus of the cured elastomer intrinsically reinforced by a two-phase design. We further demonstrated that the on-demand adhesion can be effectively used to seal joints between prefab components that are used in construction, as a prefab joint can withstand a force of at least 1000 N in a 5 cm-wide joint. Our study sheds light on the on-demand adhesion features of advanced elastomer materials and provides predominant adhesion and flexibility over regular pressure-sensitive adhesives or ductile adhesive elastomers.

Conflicts of interest

The authors declare no conflict of interest.

Acknowledgements

This work was funded by the Advanced Building Construction Initiative under the Building Technologies Office of the U.S. Department of Energy (DOE), under contract no. DE-FOA-0002099. The National Natural Science Foundation of China (grant no. 52373275) supported contributions to the writing and editing of the manuscript, as well as a few experiments. This manuscript was authored by UT-Battelle, LLC under contract no. DE-AC05-00OR22725 with the U.S. Department of Energy. The United States Government retains the publisher by accepting the article for publication, acknowledges that the United States Government retains a non-exclusive, paid-up, irrevocable, worldwide license to publish or reproduce the published form of this manuscript, or allow others to do so, for United States Government purposes. The Department of Energy will provide public access to these results of federally sponsored research in accordance with the DOE Public Access Plan (**https://energy.gov/downloads/doe-public-access-plan**).

References

1 G. Demirci, M. J. Niedźwiedź, N. Kantor-Malujdy and M. E. Fray, *Polymers*, 2022, **14**(9), 1822.
2 C. Ma, M.-G. Ma, C. Si, X.-X. Ji and P. Wan, *Adv. Funct. Mater.*, 2021, **31**(22), 2009524.
3 Y. Li, J. Li, W. Li and H. Du, *Smart Mater. Struct.*, 2014, **23**(12), 123001.
4 C. S. Luo, P. Wan, H. Yang, S. A. A. Shah and X. Chen, *Adv. Funct. Mater.*, 2017, **27**(23), 1606339.
5 Y. Guo, L. Liu, Y. Liu and J. Leng, *Adv. Intell. Syst.*, 2021, **3**(10), 2000282.
6 S. Gao, M. Zhang, C. Gainaru, A. P. Sokolov, H. Yang and P.-F. Cao, *Matter*, 2022, **5**(8), 2457–2460.
7 Q. Zhang, S. Niu, L. Wang, J. Lopez, S. Chen, Y. Cai, R. Du, Y. Liu, J.-C. Lai, L. Liu, C.-H. Li, X. Yan, C. Liu, J. B.-H. Tok, X. Jia and Z. Bao, *Adv. Mater.*, 2018, **30**(33), 1801435.
8 B. T. White and T. E. Long, *Macromol. Rapid Commun.*, 2019, **40**(1), 1800521.
9 D. Zhang, Y. Tang, X. Gong, Y. Chang and J. Zheng, *SmartMat*, 2023, e1160.
10 K. Parvathi, M. A. Al-Maghrabi, M. Subburaj and M. T. Ramesan, *Polym. Compos.*, 2021, **42**(9), 4586–4595.
11 C.-Y. Shi, Q. Zhang, C.-Y. Yu, S.-J. Rao, S. Yang, H. Tian and D.-H. Qu, *Adv. Mater.*, 2020, **32**(23), 2000345.
12 P. K. Behera, S. Mohanty and V. K. Gupta, *Polym. Chem.*, 2021, **12**(11), 1598–1621.
13 J. Huang, Y. Cai, C. Xue, J. Ge, H. Zhao and S.-H. Yu, *Nano Res.*, 2021, **14**(10), 3636–3642.
14 T. E. Long and J. Scheirs, *Modern Polyesters: Chemistry and Technology of Polyesters and Copolyesters*, John Wiley & Sons, 2005.

15 Y. Xue, J. Lin, T. Wan, Y. Luo, Z. Ma, Y. Zhou, B. T. Tuten, M. Zhang, X. Tao and P. Song, *Adv. Sci.*, 2023, 2207268.
16 Y. Lai, X. Kuang, P. Zhu, M. Huang, X. Dong and D. Wang, *Adv. Mater.*, 2018, **30**(38), 1802556.
17 X. Zhou, L. Wang, Z. Wei, G. Weng and J. He, *Adv. Funct. Mater.*, 2019, **29**(34), 1903543.
18 J. H. Koo, D. C. Kim, H. J. Shim, T.-H. Kim and D.-H. Kim, *Adv. Funct. Mater.*, 2018, **28**(35), 1801834.
19 L.-J. Yin, Y. Zhao, J. Zhu, M. Yang, H. Zhao, J.-Y. Pei, S.-L. Zhong and Z.-M. Dang, *Nat. Commun.*, 2021, **12**(1), 4517.
20 E. Siéfert, E. Reyssat, J. Bico and B. Roman, *Nat. Mater.*, 2019, **18**(1), 24–28.
21 A. M. Hubbard, W. Cui, Y. Huang, R. Takahashi, M. D. Dickey, J. Genzer, D. R. King and J. P. Gong, *Matter*, 2019, **1**(3), 674–689.
22 Y. Yang, W. Zhan, R. Peng, C. He, X. Pang, D. Shi, T. Jiang and Z. Lin, *Adv. Mater.*, 2015, **27**(41), 6376–6381.
23 S. Liu, S. Wang, S. Xuan, S. Zhang, X. Fan, H. Jiang, P. Song and X. Gong, *ACS Appl. Mater. Interfaces*, 2020, **12**(13), 15675–15685.
24 J. Kang, D. Son, G.-J. N. Wang, Y. Liu, J. Lopez, Y. Kim, J. Y. Oh, T. Katsumata, J. Mun, Y. Lee, L. Jin, J. B.-H. Tok and Z. Bao, *Adv. Mater.*, 2018, **30**(13), 1706846.
25 Z. Zhang, N. Ghezawi, B. Li, S. Ge, S. Zhao, T. Saito, D. Hun and P.-F. Cao, *Adv. Funct. Mater.*, 2021, **31**(4), 2006298.
26 J. Luo, Z. Demchuk, X. Zhao, T. Saito, M. Tian, A. P. Sokolov and P.-F. Cao, *Matter*, 2022, **5**(5), 1391–1422.
27 Z. Xu, L. Chen, L. Lu, R. Du, W. Ma, Y. Cai, X. An, H. Wu, Q. Luo, Q. Xu, Q. Zhang and X. Jia, *Adv. Funct. Mater.*, 2021, **31**(1), 2006432.
28 R. Du, Z. Xu, C. Zhu, Y. Jiang, H. Yan, H.-C. Wu, O. Vardoulis, Y. Cai, X. Zhu, Z. Bao, Q. Zhang and X. Jia, *Adv. Funct. Mater.*, 2020, **30**(7), 1907139.
29 Y. Chen, Z. Tang, X. Zhang, Y. Liu, S. Wu and B. Guo, *ACS Appl. Mater. Interfaces*, 2018, **10**(28), 24224–24231.
30 Y. Chen, Z. Tang, Y. Liu, S. Wu and B. Guo, *Macromolecules*, 2019, **52**(10), 3805–3812.
31 P. Wei and E. B. Pentzer, *Matter*, 2022, **5**(8), 2479–2481.
32 P. Song and H. Wang, *Adv. Mater.*, 2020, **32**(18), 1901244.
33 Q. Ma, S. Liao, Y. Ma, Y. Chu and Y. Wang, *Adv. Mater.*, 2021, **33**(36), 2102096.
34 D. Zhang, Y. Tang, Y. Zhang, F. Yang, Y. Liu, X. Wang, J. Yang, X. Gong and J. Zheng, *J. Mater. Chem. A*, 2020, **8**(39), 20474–20485.
35 F. Sun, Z. Li, S. Gao, Y. He, J. Luo, X. Zhao, D. Yang, T. Gao, H. Yang and P.-F. Cao, *ACS Appl. Mater. Interfaces*, 2022, **14**(22), 26014–26023.
36 X. Chu, R. Wang, H. Zhao, M. Kuang, J. Yan, B. Wang, H. Ma, M. Cui and X. Zhang, *ACS Appl. Mater. Interfaces*, 2022, **14**(14), 16631–16640.
37 K. Guk, G. Han, J. Lim, K. Jeong, T. Kang, E.-K. Lim and J. Jung, *Nanomaterials*, 2019, **9**(6), 813.
38 Y. Fang and J. Xia, *ACS Appl. Mater. Interfaces*, 2022, **14**(33), 38398–38408.
39 N. Sato, A. Murata, T. Fujie and S. Takeoka, *Soft Matter*, 2016, **12**(45), 9202–9209.
40 L. Meng, J. He and C. Pan, *Materials*, 2022, **15**(7), 2548.
41 A. B. Croll, N. Hosseini and M. D. Bartlett, *Adv. Mater. Technol.*, 2019, **4**(8), 1900193.
42 R. Coulson, C. J. Stabile, K. T. Turner and C. Majidi, *Soft Rob.*, 2022, **9**(2), 189–200.
43 H. Iwasaki, F. Lefevre, D. D. Damian, E. Iwase and S. Miyashita, *IEEE Rob. Autom. Lett.*, 2020, **5**(2), 2015–2022.
44 Z. Ma, G. Bao and J. Li, *Adv. Mater.*, 2021, **33**(24), 2007663.
45 M. Runciman, A. Darzi and G. P. Mylonas, *Soft Robot.*, 2019, **6**(4), 423–443.
46 J. Chen, J. Liu, T. Thundat and H. Zeng, *ACS Appl. Mater. Interfaces*, 2019, **11**(20), 18720–18729.
47 M. W. M. Tan, G. Thangavel and P. S. Lee, *Adv. Funct. Mater.*, 2021, **31**(34), 2103097.
48 L. Wang, Y. Wang, S. Yang, X. Tao, Y. Zi and W. A. Daoud, *Nano Energy*, 2022, **91**, 106611.
49 S. H. Jeong, S. Zhang, K. Hjort, J. Hilborn and Z. Wu, *Adv. Mater.*, 2016, **28**(28), 5830–5836.
50 C.-H. Lin, C.-Y. Huang, J.-Y. Ho and H.-Y. Hsueh, *ACS Appl. Mater. Interfaces*, 2020, **12**(19), 22365–22377.
51 B. J. Blaiszik, S. L. B. Kramer, S. C. Olugebefola, J. S. Moore, N. R. Sottos and S. R. White, *Annu. Rev. Mater. Res.*, 2010, **40**(1), 179–211.
52 D. Y. Zhu, M. Z. Rong and M. Q. Zhang, *Prog. Polym. Sci.*, 2015, **49–50**, 175–220.
53 K. Wazarkar, D. Patil, A. Rane, D. Balgude, M. Kathalewar and A. Sabnis, *RSC Adv.*, 2016, **6**(108), 106964–106979.
54 V. Nedovic, A. Kalusevic, V. Manojlovic, S. Levic and B. Bugarski, *Procedia Food Sci.*, 2011, **1**, 1806–1815.
55 C. J. Martínez Rivas, M. Tarhini, W. Badri, K. Miladi, H. Greige-Gerges, Q. A. Nazari, S. A. Galindo Rodríguez, R. Á. Román, H. Fessi and A. Elaissari, *Int. J. Pharm.*, 2017, **532**(1), 66–81.
56 M. Villiou, J. I. Paez and A. del Campo, *ACS Appl. Mater. Interfaces*, 2020, **12**(34), 37862–37872.
57 W. Sliwka, *Angew. Chem., Int. Ed. Engl.*, 1975, **14**(8), 539–550.
58 Q. Lu, Z. Yang, X. Meng, Y. Yue, M. A. Ahmad, W. Zhang, S. Zhang, Y. Zhang, Z. Liu and W. Chen, *Adv. Funct. Mater.*, 2021, **31**(23), 2100151.
59 S. M. Jee, C.-H. Ahn, J. H. Park, T. A. Kim and M. Park, *Composites, Part B*, 2020, **202**, 108438.
60 M. M. Caruso, B. J. Blaiszik, S. R. White, N. R. Sottos and J. S. Moore, *Adv. Funct. Mater.*, 2008, **18**(13), 1898–1904.
61 S. H. Cho, H. M. Andersson, S. R. White, N. R. Sottos and P. V. Braun, *Adv. Mater.*, 2006, **18**(8), 997–1000.
62 M. J. Shin, Y. J. Shin, S. W. Hwang and J. S. Shin, *J. Appl. Polym. Sci.*, 2013, **129**(3), 1036–1044.
63 Y. Zhang, J. Yu, H. N. Bomba, Y. Zhu and Z. Gu, *Chem. Rev.*, 2016, **116**(19), 12536–12563.
64 J. Giro-Paloma, C. Barreneche, M. Martínez, B. Šumiga, A. I. Fernández and L. F. Cabeza, *Renewable Energy*, 2016, **85**, 732–739.
65 H. Zhao, X. Fei, L. Cao, B. Zhang and X. Liu, *Materials*, 2019, **12**(3), 393.
66 A. Ghaemi, A. Philipp, A. Bauer, K. Last, A. Fery and S. Gekle, *Chem. Eng. Sci.*, 2016, **142**, 236–243.

67 A. P. Esser-Kahn, S. A. Odom, N. R. Sottos, S. R. White and J. S. Moore, *Macromolecules*, 2011, **44**(14), 5539–5553.
68 J. Yang, M. W. Keller, J. S. Moore, S. R. White and N. R. Sottos, *Macromolecules*, 2008, **41**(24), 9650–9655.
69 P.-F. Cao, B. Li, T. Hong, K. Xing, D. N. Voylov, S. Cheng, P. Yin, A. Kisliuk, S. M. Mahurin, A. P. Sokolov and T. Saito, *ACS Appl. Mater. Interfaces*, 2017, **9**(31), 26483–26491.
70 T. Yin, M. Z. Rong, M. Q. Zhang and G. C. Yang, *Compos. Sci. Technol.*, 2007, **67**(2), 201–212.
71 J. S. Nakka, K. M. B. Jansen and L. J. Ernst, *J. Polym. Res.*, 2011, **18**(6), 1879–1888.
72 G. Yang, S.-Y. Fu and J.-P. Yang, *Polymer*, 2007, **48**(1), 302–310.
73 E. Urbaczewski-Espuche, J. Galy, J.-F. Gerard, J.-P. Pascault and H. Sautereau, *Polym. Eng. Sci.*, 1991, **31**(22), 1572–1580.
74 S. J. McCarthy, G. F. Meijs, N. Mitchell, P. A. Gunatillake, G. Heath, A. Brandwood and K. Schindhelm, *Biomaterials*, 1997, **18**(21), 1387–1409.
75 M. Strankowski, D. Włodarczyk, Ł. Piszczyk and J. Strankowska, *J. Spectrosc.*, 2016, **2016**, 7520741.
76 Z. Wen, M. K. McBride, X. Zhang, X. Han, A. M. Martinez, R. Shao, C. Zhu, R. Visvanathan, N. A. Clark, Y. Wang, K. Yang and C. N. Bowman, *Macromolecules*, 2018, **51**(15), 5812–5819.
77 V. A. Gabriel and M. A. Dubé, *Macromol. React. Eng.*, 2019, **13**(2), 1800057.
78 M. Tang, P. Zheng, K. Wang, Y. Qin, Y. Jiang, Y. Cheng, Z. Li and L. Wu, *J. Mater. Chem. A*, 2019, **7**(48), 27278–27288.
79 J. Li, A. Celiz, J. Yang, Q. Yang, I. Wamala, W. Whyte, B. Seo, N. Vasilyev, J. Vlassak and Z. Suo, *Science*, 2017, **357**(6349), 378–381.
80 D. F. S. Saldanha, C. Canto, L. F. M. da Silva, R. J. C. Carbas, F. J. P. Chaves, K. Nomura and T. Ueda, *Int. J. Adhes. Adhes.*, 2013, **47**, 91–98.
81 L. Wang, G. Gao, Y. Zhou, T. Xu, J. Chen, R. Wang, R. Zhang and J. Fu, *ACS Appl. Mater. Interfaces*, 2019, **11**(3), 3506–3515.
82 J. S. Santana, E. S. Cardoso, E. R. Triboni and M. J. Politi, *Polymers*, 2021, **13**(24), 4393.
83 J. D. Ferry, *Viscoelastic Properties of Polymers*, John Wiley & Sons, 1980.
84 T. Hwang, Z. Frank, J. Neubauer and K. J. Kim, *Sci. Rep.*, 2019, **9**(1), 9658.
85 M. Hao, L. Li, S. Wang, F. Sun, Y. Bai, Z. Cao, C. Qu and T. Zhang, *Microsyst. Nanoeng.*, 2019, **5**(1), 9.
86 T. Noguchi, M. Endo, K. Niihara, H. Jinnai and A. Isogai, *Compos. Sci. Technol.*, 2020, **188**, 108005.
87 B. M. Boyle, O. Heinz, G. M. Miyake and Y. Ding, *Macromolecules*, 2019, **52**(9), 3426–3434.
88 B. D. B. Tiu, P. Delparastan, M. R. Ney, M. Gerst and P. B. Messersmith, *Angew. Chem., Int. Ed.*, 2020, **59**(38), 16616–16624.
89 A. Zosel, *J. Adhes.*, 1989, **30**(1–4), 135–149.
90 T. L. Gordon and M. E. Fakley, *Int. J. Adhes. Adhes.*, 2003, **23**(2), 95–100.
91 F. P. M. Mercx, A. Benzina, A. D. van Langeveld and P. J. Lemstra, *J. Mater. Sci.*, 1993, **28**(3), 753–759.
92 Z. Zhang, J. Luo, S. Zhao, S. Ge, J.-M. Y. Carrillo, J. K. Keum, C. Do, S. Cheng, Y. Wang, A. P. Sokolov and P.-F. Cao, *Matter*, 2022, **5**(1), 237–252.
93 Y. Zheng, R. Kiyama, T. Matsuda, K. Cui, X. Li, W. Cui, Y. Guo, T. Nakajima, T. Kurokawa and J. P. Gong, *Chem. Mater.*, 2021, **33**(9), 3321–3334.
94 Y. Zhuo, Z. Xia, Y. Qi, T. Sumigawa, J. Wu, P. Šesták, Y. Lu, V. Håkonsen, T. Li, F. Wang, W. Chen, S. Xiao, R. Long, T. Kitamura, L. Li, J. He and Z. Zhang, *Adv. Mater.*, 2021, **33**(23), 2008523.
95 S. Sun, M. Li and A. Liu, *Int. J. Adhes. Adhes.*, 2013, **41**, 98–106.
96 S. Mapari, S. Mestry and S. T. Mhaske, *Polym. Bull.*, 2021, **78**(7), 4075–4108.
97 R. Jovanović and M. A. Dubé, *J. Macromol. Sci., Part C*, 2004, **44**(1), 1–51.
98 B. T. Poh and H. K. Kwo, *Polym.-Plast. Technol. Eng.*, 2007, **46**(10), 1021–1024.
99 B. T. Poh and H. K. Kwo, *J. Appl. Polym. Sci.*, 2007, **105**(2), 680–684.
100 I. Khan and B. T. Poh, *J. Polym. Environ.*, 2011, **19**(3), 793–811.
101 S. G. Naoum, *Int. J. Prod. Perform. Manage.*, 2016, **65**(3), 401–421.
102 K. M. A. El-Abidi and F. E. M. Ghazali, *Appl. Mech. Mater.*, 2015, **802**, 668–675.
103 F. E. Boafo, J.-H. Kim and J.-T. Kim, *Sustainability*, 2016, **8**(6), 558.